

Synthesis, Spectral Characterization, Thermal Investigation, Computational Studies, Molecular Docking, and *In Vitro* Biological Activities of a New Schiff Base Derived from 2-Chloro Benzaldehyde and 3,3'-Dimethyl-[1,1'-biphenyl]-4,4'-diamine

Priteshkumar M. Thakor, Rajesh J. Patel, Ranjan Kr. Giri, Sunil H. Chaki, Ankurkumar J. Khimani, Yati H. Vaidya, Parth Thakor, Anjali B. Thakkar, and Jatin D. Patel*

Cite This: *ACS Omega* 2023, 8, 33069–33082

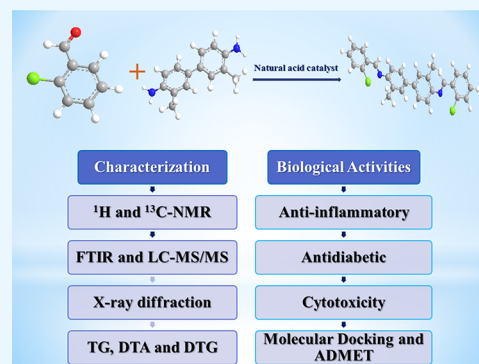
Read Online

ACCESS |

Metrics & More

Article Recommendations

ABSTRACT: The current research involves the synthesis of a new Schiff base through the reaction between 2-chlorobenzaldehyde and 3,3'-dimethyl-[1,1'-biphenyl]-4,4'-diamine by using a natural acid catalyst and a synthesized compound physicochemically characterized by X-ray diffraction, Fourier transform infrared spectroscopy, ^1H - and ^{13}C -nuclear magnetic resonance, and liquid chromatography–mass spectrometry. Thermal studies were conducted using thermogravimetric, differential thermal analysis, and differential thermogravimetric curves. These curves were obtained in an inert nitrogen environment from ambient temperature to 1263 K using heating rates of 10, 15, and 20 $\text{K}\cdot\text{min}^{-1}$. Using thermocurve data, model-free isoconversional techniques such as Kissinger–Akahira–Sunose, Flynn–Wall–Ozawa, and Friedman are used to determine kinetic parameters. These parameters include activation energy, phonon frequency factor, activation enthalpy, activation entropy, and Gibb's free energy change. All of the results have been thoroughly investigated. The molecule's anti-inflammatory and antidiabetic properties were also examined. To learn more about the potential of the Schiff base and how successfully it can suppress the amylase enzyme, a molecular docking experiment was also conducted. For *in silico* research, the Swiss Absorption, Distribution, Metabolism, Excretion, and Toxicity algorithms were used to calculate the theoretical pharmacokinetic properties, oral bioavailability, toxic effects, and biological activities of the synthesized molecule. Moreover, the cytotoxicity tests against a human lung cancer cell line (A549) using the 3-(4,5-dimethylthiazol-2-yl)-2,5-diphenyltetrazolium bromide assay demonstrated that the synthesized Schiff base exhibited significant anticancer properties.



1. INTRODUCTION

Schiff bases are nitrogen analogs of aldehydes and ketones, with imine or azomethine groups replacing the carbonyl group ($-\text{C}=\text{O}$). Schiff bases are used in closure, cycloaddition, and replacement to synthesize several beneficial compounds for industry and human health.^{1–3} They are also analgesics, anti-inflammatory agents, allergy inhibitors, radical scavengers, anticancer agents, antibacterial agents, antidiabetic agents, and antioxidants.^{4–7} Due to their biological uses, simplicity of synthesis, chelating properties, and stability, Schiff base compounds are an important and extensively studied class.^{8–10}

The rapid growth of pharmaceutical and medicinal chemistry has redirected researchers' attention to drug development, even for complex disorders like diabetes mellitus.¹¹ Abnormal production of insulin is the underlying cause of diabetes mellitus, which is recognized as a critical global health issue. Schiff bases have shown some interesting results in several types of research to examine insulin-mimetic

qualities.¹² For example, Szklarzewick's group demonstrated the antidiabetic potentiality of a Schiff base.¹³

Cancer is a hard disease to deal with all over the world for several reasons. One of the biggest problems with getting rid of cancer is that it can become resistant to the drugs used to treat it.^{14–16} The rate at which cancer responds to cytotoxic drugs is not good enough. Researchers are trying to find a new drug, which has made them think about new agents with less systemic toxicity and better cytotoxicity.¹⁷ Furthermore, numerous papers described the anticancer effects of Schiff bases employing a range of human tumor cell lines.¹⁸

Received: July 20, 2023

Accepted: August 15, 2023

Published: August 25, 2023



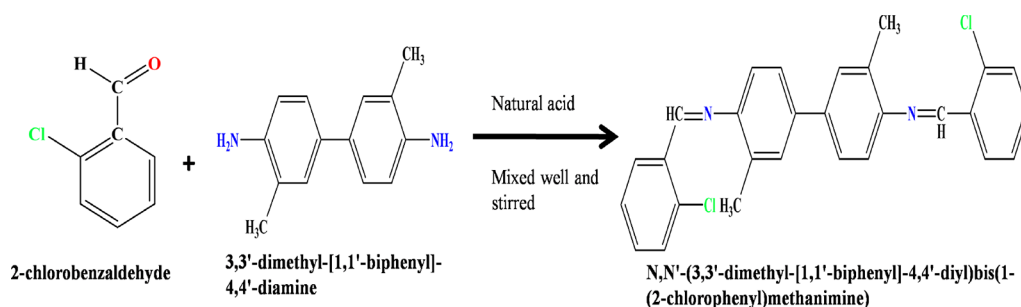


Figure 1. Synthesis pathway of the Schiff base.

The function of inflammation in human and animal diseases has drawn global interest. Inflammatory disorders are responsible for causing numerous diseases.^{19,20} Synthesizing and developing novel and more potent anti-inflammatory drugs with no or fewer side effects are crucial due to the side effects of existing drugs that have caused serious clinical issues.²¹ Schiff bases have an azomethine linkage, which has sparked the interest of pharmacists due to its predicted efficiency.²² In light of Schiff bases' potential as a pharmacophore in numerous pharmacologically active medications, it was decided to synthesize them and investigate their anti-inflammatory, antidiabetic, and anticancer effects.²³

The utilization of natural biocatalysts is becoming increasingly prevalent in various fields of chemistry.^{24–26} We therefore examined the synthesis, structural traits, and kinetic parameters of the Schiff base made from 2-chlorobenzaldehyde and 3,3'-dimethyl-[1,1'-biphenyl]-4,4'-diamine by using a natural acid catalyst in the current work. The chelation potential of Schiff bases depends upon the presence of more than one donor site that may promote the formation of a stable ring-like structure. As a result of this condition, it is not feasible to generate complex combinations of the Schiff base that was synthesized in this study. The synthesized compound was characterized using liquid chromatography–mass spectrometry (LC–MS/MS), ¹H- and ¹³C-nuclear magnetic resonance (NMR), Fourier transform infrared spectroscopy (FTIR), and X-ray diffraction (XRD). Thermogravimetric (TG), differential thermal analysis (DTA), and differential thermogravimetric (DTG) curves were collected in a nitrogen atmosphere to assess the product's thermal properties.^{27–29} Additionally, the anti-inflammatory property of Schiff base was examined *in vitro* using the albumin denaturation bioassay. The ability to suppress α -amylase *in vitro* and by molecular docking was also evaluated. In the *in silico* research, the Swiss Absorption, Distribution, Metabolism, Excretion, and Toxicity (ADMET) algorithms were employed to estimate the theoretical pharmacokinetic properties, oral bioavailability, toxic effects, and biological activities of the synthesized molecule.³⁰ Computer projections show that it might work as an enhancer of membrane permeability. Using the human lung cancer cell line (A549), the *in vitro* cytotoxicity of synthesized Schiff base was assessed using the “3-(4,5-dimethylthiazol-2-yl)-2,5-diphenyltetrazolium bromide” (MTT) assay.^{31,32} The findings demonstrated that the synthesized Schiff base exhibits good cytotoxicity for a human lung cancer cell line (A549).

2. MATERIALS AND METHODS

2.1. Materials. The following materials were used to produce Schiff base: *o*-chloro benzaldehyde [minimum assay

98%, Sigma Aldrich] and 3,3'-dimethyl-[1,1'-biphenyl]-4,4'-diamine [minimum assay 97.5%, Spectrochem]; all of the compounds were of analytical grade and were employed directly after delivery without further purification. All the solvents used were purchased from Merck, Loba, SRL, and Spectrochem, and they were distilled before use. For freshly prepared lemon juice, the lemons were bought from the nearby market.

2.2. Instrumental Methods. By using the Rigaku Ultima IV Powder X-ray diffractometer (XRD) and $\lambda_{\text{CuK}\alpha} = 1.542 \text{ \AA}$ (X-ray), the unit crystal structure of the produced product was identified for its physicochemical characterization. The FTIR spectrum was recorded using a PerkinElmer FTIR L160000T spectrometer. Analab's melting point apparatus was used to determine the melting point of the synthesized Schiff base, and thin-layer chromatography (TLC) analysis was used to determine the progress of the reaction. The JEOL ECZ600R at 600 MHz was used to record the ¹H-NMR and ¹³C-NMR spectra using THF or DMSO-*d*₆ as a solvent. The MS spectrum was recorded using a Shimadzu LC–MS/MS 8050. The Seiko SII-EXSTAR TG/DTA-7200 thermal analyzer was used to record the thermogravimetric (TG), differential thermal analysis (DTA), and differential thermogravimetric (DTG) curves.

2.3. General Procedure for the Synthesis of N,N'-(3,3'-Dimethyl-[1,1'-biphenyl]-4,4'-diyl) bis(1-(2-chlorophenyl) methanimine).³³ 2-Chlorobenzaldehyde (10 mmol, 1.41 g) was dissolved in a minimal volume of absolute ethanol, and this solution was added drop by drop to a beaker containing a solution of 5-mmol (1.06 g) of 3,3'-dimethyl-[1,1'-biphenyl]-4,4'-diamine in ethanol. Then, 2 mL of lemon juice was added to the reaction mixture while stirring continuously. The reaction mixture was stirred continuously at room temperature, and TLC was used to record the development of the reaction. Here, the reactants are taken in a 2:1 molar ratio. The result was a solid, lime-colored product that was filtered, ethanol-washed, and recrystallized with dimethyl sulfoxide (DMSO). The final product was obtained in a yield of 2.04 g. By dissolving the Schiff base in DMSO and stirring the mixture, a homogeneous lime-colored solution was prepared. Over a period of at least 2 months, no discernible change in color was observed, indicating the solution's remarkable stability. Figure 1 depicts the synthetic pathway of the Schiff base.

2.4. Biological Activities of N,N'-(3,3'-Dimethyl-[1,1'-biphenyl]-4,4'-diyl) bis(1-(2-chlorophenyl) methanimine). **2.4.1. Anti-Inflammatory Activity.** The present study examined the anti-inflammatory properties of a synthetic compound through the implementation of the albumin denaturation inhibition technique, which has been previously

investigated following references with slight modifications.^{34–36} The reaction mixture contained a solution of Schiff base in the concentration range of 100–500 $\mu\text{g}/\text{mL}$ and a 1% aqueous solution of bovine albumin fraction. The pH of the reaction mixture was slightly elevated through the addition of a small quantity of 1 N hydrochloric acid. The reaction mixtures underwent preheating at 37 °C for 20 min, followed by additional preheating at 51 °C for another 20 min. After the cooling of the samples, their turbidity was assessed at a wavelength of 660 nm. The experiment was replicated three times. The percentage of protein denaturation inhibition was determined using the formula as follows:

$$\% \text{ inhibition} = \frac{\text{absorbance value of control} - \text{absorbance value of test}}{\text{absorbance value of control}} \times 100 \quad (1)$$

2.4.2. α -Amylase Inhibitory Activity. The experiment involving *in vitro* amylase inhibition was conducted utilizing methods.^{37–39} A 0.5 mL volume of Schiff base solution with a concentration of 1 mg/mL was introduced into the amylase enzyme solution that was previously prepared in a 0.1 M phosphate buffer with a pH of 6.9 during an enzyme reaction. Following a 10 min incubation period at a temperature of 25 °C, a 0.5 mL volume of a 1% starch solution in 0.1 M phosphate buffer with a pH of 6.8 was introduced. Furthermore, the reaction mixture was maintained at a temperature of 25 °C for 10 min. For the control, the same procedure was employed, with the exception that 0.5 mL of buffer was used in place of the enzyme solution. Following a 10 min incubation period, the dinitrosalicylic acid reagent was introduced to both the control and test reactions. Subsequently, both reactions were subjected to an additional 10 min incubation period in a boiling water bath. The absorbance at 540 nm was measured using a UV–visible spectrophotometer after the cooling of the reaction mixture. The inhibition percentage of the α -amylase enzyme was determined utilizing the following formula:

$$\% \text{ inhibition} = \frac{\text{absorbance value of control} - \text{absorbance value of test}}{\text{absorbance value of control}} \times 100 \quad (2)$$

2.5. Molecular Docking Study. With the aid of Auto Dock Vina,⁴⁰ the protein–ligand complexes were molecularly docked. The RCSB Protein Data Bank (PDB ID: 4X9Y) was used to download the crystallographic 3D structure of Wild-Type Human Pancreatic Alpha-Amylase, which was then prepared in AutoDockTools 1.5.6⁴¹ by removing water and solvent molecules, removing the bound ligand, adding polar hydrogen, and partially assigning charges. Auto Dock PDBQT format was used to save the produced structure. ChemBio3D Ultra 14.0⁴² was used to optimize the synthesized Schiff base (SB) and reference medication (acarbose). The Merck Molecular Force Field (MMFF94) technique⁴³ was used to optimize the structural properties of SB and acarbose. Using AutoDockTools 1.5.6, the mol2 format of the ligand was further converted to the PDBQT file. Ultimately, the docking process for this ligand model was examined. To determine the mechanism of the macromolecular targets' binding to the tiny active components, molecule docking was used. The Lamarckian genetic algorithm's default settings were used to dock the product in this case. The Auto Grid settings for the

receptor were as follows: grid size: $X = 40$, $Y = 40$, and $Z = 40$; grid center: $X = -8.289$, $Y = -5.639$, and $Z = 15.835$; grid spacing: 0.375 Å. Free binding energy was used to quantify the findings. The distance between a certain atom or molecule and the amino acids was determined using the Biovia Discovery Studio Visualizer.

2.6. In Silico Analysis. **2.6.1. Prediction of Biological Activities.** The activity forecast of Schiff base was assessed using the PASS online tools. To estimate the biological applicability of an organic compound, the structure of the molecule of concern can be compared with a database (<https://www.way2drug.com/passonline/>) of various known organic molecules with established biological activities. The active or inactive status, as described in terms of their respective probabilities, Pa or Pi, of an organic molecule targeting a biological point can be assessed using the PASS tool.^{44,45} The biological activity of ciprofloxacin was evaluated as a comparative. Ciprofloxacin, a second-generation broad-spectrum fluoroquinolone, was chosen as the standard drug due to its approval by the U.S. Food and Drug Administration (FDA) for treating and preventing various infections caused by specific bacteria. These infections include certain urinary tract infections, lower respiratory tract infections, and skin infections. The mechanism of action of ciprofloxacin involves its interaction with bacterial topoisomerases, resulting in the generation of oxidative radicals and subsequent bacterial cell death.

2.6.2. Prediction of Oral Bioavailability. The Swiss ADME⁴⁶ program (<http://www.swissadme.ch/index.php#>) was employed for calculating the oral bioavailability of the synthesized compound's theoretical values. For comparison, the oral bioavailability of ciprofloxacin was investigated. Calculations were made for the chemical's total polar surface area (TPSA), partition coefficient (water/oil) (iLogP), molecular weight, number of hydrogen acceptors (nALH), number of donors (nDLH), and other properties. A molecule of concern must meet the requirements for a minimum of three factors under research to obtain an accurate estimate of oral bioavailability: molecular weight of 500 Da, nALH, nDLH, TPSA 140 Å², and LogP.⁴⁷

2.6.3. Estimation of the Toxic Effects and Pharmacokinetic Properties. The Swiss ADMET (<https://admet.scbdd.com/calcpre/index/#>) programs were used to explore the possible harmful effects of Schiff base, as well as theoretical values of pharmacokinetic properties (absorption and then distribution followed by metabolism and then excretion). The Swiss ADMET (<https://admet.scbdd.com/calcpre/index/#>) online predictor was used to analyze a variety of properties of the synthesized compound, including absorption through the gastrointestinal route, clearance of the blood–brain barrier, and permeation through the skin (log Kp in centimeters \times sec⁻¹). The log Kp indicates how permeable the molecule is to the skin. Merging the obtained values of iLogP, its likeliness as a drug and its solubility (Log S; higher solubility is represented by the closeness of its value to zero) along with molar mass, and last, the toxicity as a singular value of concern, the possibility of Schiff base becoming a commercially available medicine (“drug score”) was calculated by the Osiris program (www.organic-chemistry.org/prog/peo/drugScore.html). As a measure of commercialization suitability, 0.1 to 1.0 drug scores were considered.⁴⁸

2.7. In Vitro Cytotoxicity Study. **2.7.1. Cell Culture and Cell Line.** A human lung cancer cell line (A549) was made

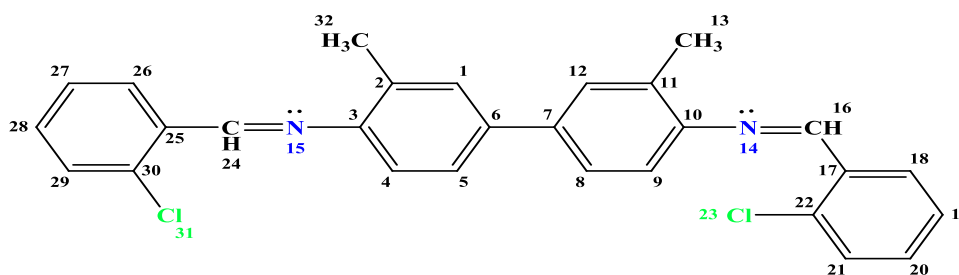


Figure 2. Structure of *N,N'*-(3, 3'-dimethyl-[1,1'-biphenyl]-4,4'-diyl) bis(1-(2-chlorophenyl) methanimine).

available by the NCCS in Pune, India. Gibco, Invitrogen, CA, USA, provided DMEM/F12, fetal bovine serum, 50 $\mu\text{g}/\text{mL}$ penicillin, and 50 $\mu\text{g}/\text{mL}$ streptomycin. The cell line was grown in a monolayer in DMEM/F12 media with 10% fetal bovine serum, 50 $\mu\text{g}/\text{mL}$ penicillin, and 50 $\mu\text{g}/\text{mL}$ streptomycin at 37 $^{\circ}\text{C}$ in a humidified environment of 5% carbon dioxide.⁴⁹ The media were changed every 3 days up until confluence was reached by the cells. The cells were then sub-cultured at that moment.

2.7.2. Antiproliferative Test. Gajera et al.'s method,⁵⁰ with a few tweaks, was used to conduct an antiproliferative assay to look at the biocompatibility of the Schiff base. To get the correct concentrations, culture media were diluted using water after a Schiff base was added to it. Each batch of chemical solutions was prepared immediately prior to usage. Ninety-six-well plates with the full medium were filled with exponentially growing cells (10,000 cells per well), and they were then incubated for 24 h. Cells were exposed to various concentrations of all test nanoparticles after the initial incubation, and they were then incubated for an additional 24 h. Afterward, 5 μL of MTT (5 mg/mL) was added into the treated cells in a separate well, and the cells were then cultivated for 3–4 h at 37 $^{\circ}\text{C}$ in a CO_2 incubator to produce Formazan crystals and create a purplish color. The culture (100 μL) was mixed with 100 μL of tissue culture-grade DMSO, filled in each well, and incubated in the medium. A microplate reader was used to determine the final suspension's absorbance at 570 nm. As a negative control, wells with complete media, nanoparticles, and MTT reagents were employed. Using the provided formula, the optical density (OD) readings from an antiproliferative assay were utilized to quantify cell viability.

$$\% \text{ cell viability} = \frac{\text{absorbance value for sample nanoparticle} - \text{treated cells}}{\text{absorbance value of control cells}} \times 100 \quad (3)$$

$$\% \text{ cell inhibition} = (100 - \% \text{ cell viability}) \quad (4)$$

3. RESULTS AND DISCUSSION

The synthesized product's IUPAC (International Union of Pure and Applied Chemistry) name is determined to be *N,N'*-(3, 3'-dimethyl-[1,1'-biphenyl]-4,4'-diyl) bis(1-(2-chlorophenyl) methanimine). Figure 2 depicts the compound's structure. It is a lime-colored crystal powder having a yield of about 89.41% by the above-discussed synthesis pathway. The product's melting point is determined to be 169 $^{\circ}\text{C}$. The as-synthesized compound is found to be soluble in tetrahydrofuran (THF), dimethyl formamide (DMF), dimethyl sulfoxide (DMSO), and dichloromethane (DCM).

3.1. Spectral Characterization of *N,N'*-(3, 3'-Dimethyl-[1,1'-biphenyl]-4, 4'-diyl) bis(1-(2-chlorophenyl) methanimine).

3.1.1. FTIR.

The synthetic compound's infrared spectrum (Figure 3) was registered between 450 and 4000

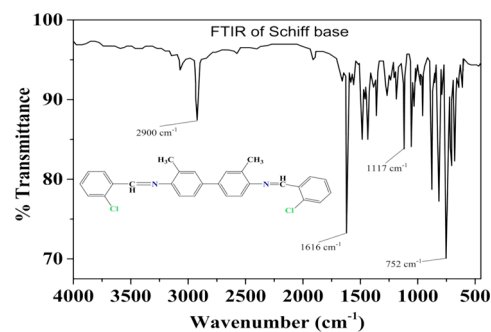


Figure 3. FTIR spectrum of the Schiff base.

cm^{-1} , revealing a band of medium absorption at 1616 cm^{-1} , which can be attributed to the $\nu(\text{C}=\text{N})$ azomethine stretching vibrations, confirming the establishment of the Schiff base linkage. The compound's spectrum lacks $\text{C}=\text{O}$ and NH_2 stretching vibrations, which are associated with aldehyde and amine, respectively, indicating the formation of imine linkage needed for the development of Schiff base.⁵¹ $\nu(\text{C}-\text{Cl})$ is accountable for the strong band seen at 752 cm^{-1} . At 1117 cm^{-1} , the $(\text{Ph}-\text{N})$ produced a medium-intensity band. The presence of aromatic $\nu(\text{C}-\text{H})$ generated the stretching vibrations around 2900 cm^{-1} .

3.1.2. $^1\text{H-NMR}$. The $^1\text{H-NMR}$ spectrum of the derived compound (Figure 4) was obtained in $\text{DMSO}-d_6$; signals seen between 8.966 and 9.002 ppm suggested alpha hydrogen for imine linkage ($\text{HC}=\text{N}$).⁵² The resonance of CH_3 is responsible for the signals in the range of 2.528–3.064 ppm.⁵³ The molecule has an aromatic ring, and the numerous signals seen in the range of 6.863–8.412 ppm are attributed to aromatic proton resonance. The other signals observed

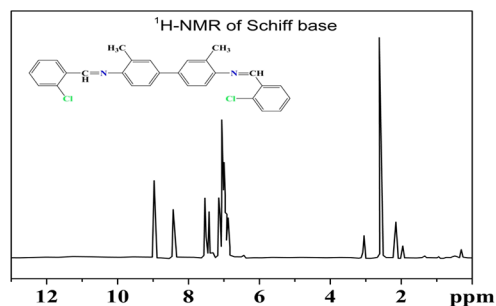


Figure 4. $^1\text{H-NMR}$ spectrum of the derived product.

between 1.937 and 2.158 are because of the resonance of the solvent.

3.1.3. $^{13}\text{C-NMR}$. The $^{13}\text{C-NMR}$ spectrum of the synthesized compound (Figure 5) was measured in $\text{DMSO-}d_6$. The carbon

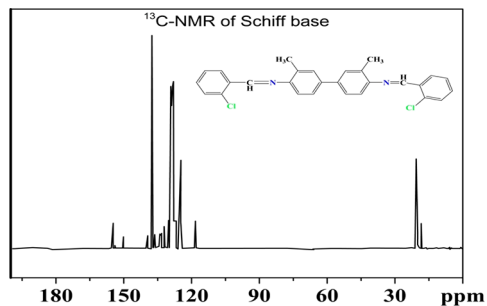


Figure 5. $^{13}\text{C-NMR}$ spectrum of the synthesized compound.

linked to the chlorine revealed signals between 136.21 and 139.38 ppm in the spectrum. The $-\text{CH}_3$ group carbon is liable for the signals observed between 18.28 and 20.98 ppm. The signals between 134.10 and 118.71 ppm indicated the existence of aromatic carbons in the benzene ring.⁵⁴ The chemical shift value of alpha carbon connected to the amine group is influenced by the presence of the imine group, which was measured at 155.01 ppm. The carbon linked to nitrogen has a chemical shift of 150.24 ppm.⁵⁵

3.1.4. *Mass Spectrum (MS)*. The synthesized product's mass spectrum was gathered and examined for validation, and it is displayed in Figure 6a. The mass spectrum of the synthesized molecule consisted of a molecular ion peak at $m/z = 458$, which agrees well with its molecular weight (457), which further supports the product's structure. The Schiff base's proposed structure and the observed peaks are in good agreement. Other prominent peaks in the mass spectrum were observed at m/z 71, 87, 186, 245, 296, 315, and 356, which are in good agreement with the proposed fragments of the

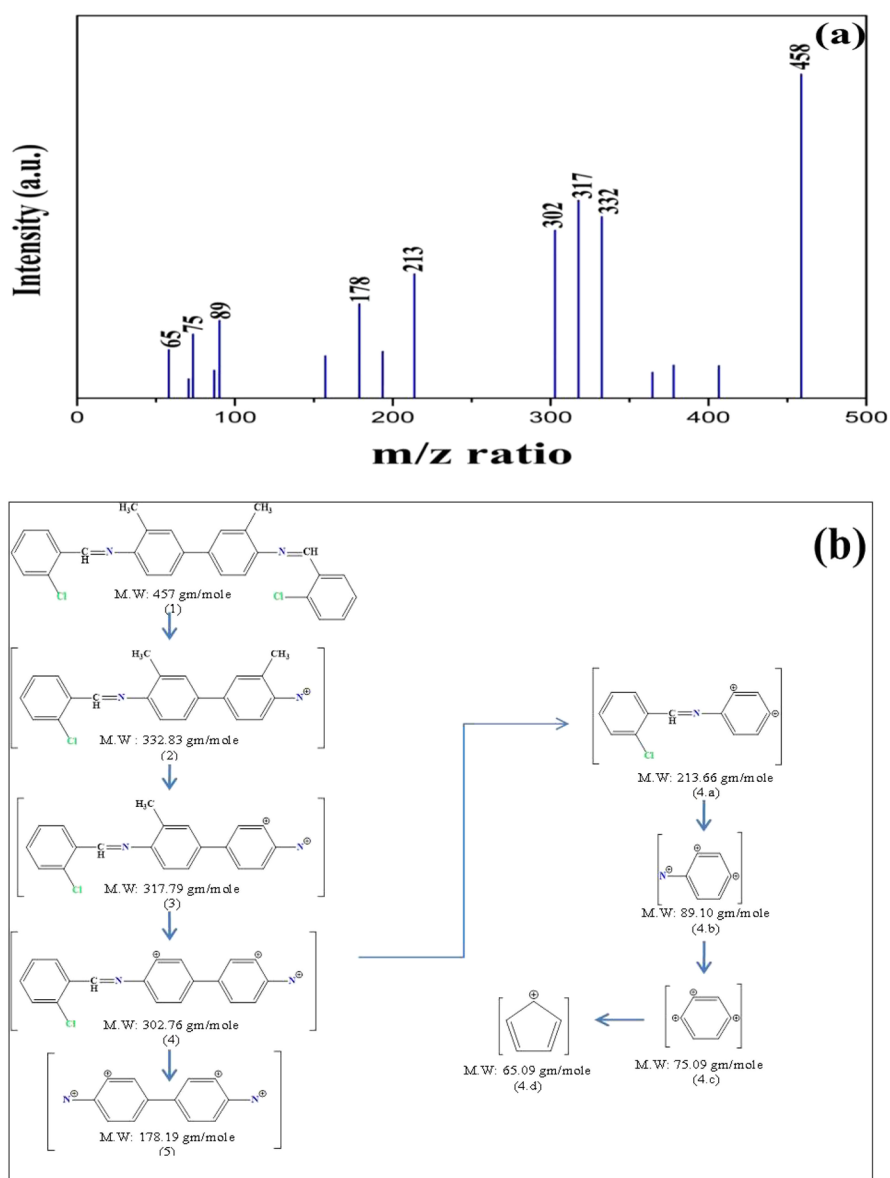


Figure 6. (a) Mass spectrum and (b) proposed mass fragmentation pattern of the developed compound.

compound shown in Figure 6b. Strong evidence for the production of Schiff base compound was supplied by the aforementioned data.

3.2. X-ray Diffraction (XRD). The only method available to identify the material's crystallographic formation and phase is XRD. It is a rapid analytical approach first and foremost used for crystalline material phase identification and can offer information on the dimensions of the unit cell. The powder of the prepared sample was analyzed for structural determination by using the Rigaku Ultima IV Powder X-ray diffractometer (XRD) and $\lambda_{\text{CuK}\alpha} = 1.542 \text{ \AA}$ (X-ray). Figure 7 shows the XRD

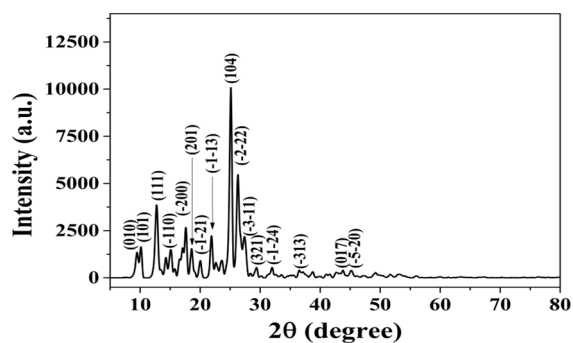


Figure 7. XRD pattern of the synthesized compound.

pattern of the Schiff base-derived product. The X-ray powder diffractometer was used to perform XRD at room temperature using Cu-K α radiation with an X-ray beam wavelength of 1.5406 nm. The 2θ range of XRD was 5° to 80° . As the synthesized compound possesses a triclinic crystal structure having lattice parameters $a = 9.56 \text{ \AA}$, $b = 9.65 \text{ \AA}$, $c = 14.76 \text{ \AA}$, $\alpha = 88.82^\circ$, $\beta = 86.82^\circ$, and $\gamma = 76.12^\circ$,⁵⁶ the XRD spectrum reveals the polycrystalline nature of as-synthesized material. The most prominent peak is observed at $2\theta = 25.11^\circ$ (1 0 4). The XRD parameters are shown in Table 1.

The typical crystallite size of the sample (in nm) is predicted using Scherrer's relation^{57,58}

$$D = \frac{k\lambda}{\beta_{hkl} \cos \theta} \quad (5)$$

Table 1. XRD Parameters of the Schiff Base-Derived Product

(h k l)	2θ	d (Å)	intensity (a.u.)
(0 1 0)	9.48	9.31	1350
(1 0 1)	10.13	8.71	1641
(1 1 1)	12.72	6.94	3867
(-1 1 0)	14.29	6.19	1077
(-2 0 0)	17.61	5.03	2672
(2 0 1)	18.57	4.77	1544
(-1 -2 1)	20.03	4.42	910
(-1 -1 3)	21.88	4.05	2223
(1 0 4)	25.11	3.54	10,111
(-2 -2 2)	26.30	3.38	5479
(-3 -1 1)	27.38	3.25	2186
(3 2 1)	29.37	3.03	545
(-1 -2 4)	31.26	2.85	156
(-3 1 3)	36.52	2.45	404
(0 1 7)	43.79	2.06	400
(-5 -2 0)	45.17	2.00	388

Here, the "k" value of the shape constant is 0.95 (organic compounds), λ is the X-ray wavelength ($\lambda_{\text{CuK}\alpha}$ is 1.5406 Å), β_{hkl} is the full-width at half maxima (FWHM) of diffraction planes/peaks, and θ is the angle of diffraction. The value of D is found to be 21.40 nm.

In addition to that, the dislocation density is determined for the as-synthesized sample. The dislocation density value is found to be $2.18 \times 10^{15} \text{ m}^{-2}$. The dislocation density is estimated through the following relation^{59,60}

$$\delta = \frac{1}{D_{\text{XRD}}^2} \quad (6)$$

δ is the dislocation density in the line of unit area.

3.3. Thermal Study. TG, DTA, and DTG thermocurves are measured simultaneously for the Schiff base (Figure 8). The thermal curves are measured at 10, 15, and 20 K·min⁻¹ heating rates in an inert N₂ atmosphere with temperatures ranging from ambient to 1263 K. TG curves of the sample in Figure 8a demonstrate that there is constant weight loss corresponding to the heating rates. Figure 8b, which depicts the simultaneous DTA curve, demonstrates that the curves begin as being endothermic before becoming exothermic. The initial endothermic nature indicates that both hydrous and loosely connected groups absorb heat and are lost.⁶¹ It can be seen from weight loss in TG curves that the sample is decomposing at high temperatures with an exothermic character later on (Figure 8a). The kinetic parameters are estimated from the single and sharp decomposition peak in the DTG thermocurve as shown in Figure 8c. Table 2 lists the weight loss (%) for each heating rate.

Table 2 reveals that when the heating rate rises, the sample's overall weight loss also rises. The larger weight loss seen at higher heating rates can be attributed to the more random heating of the samples. The sample is heated unevenly, which causes additional decomposition of the sample. When the heating rate is lower, the investigated sample's heat dissipation is uniform. When opposed to uneven heat dissipation, homogeneous heat dissipation causes less weight loss.

3.4. Kinetic Analysis. Kinetic parameters are estimated using isoconversional linear approaches such as Kissinger–Akahira–Sunose (KAS), Flynn–Wall–Ozawa (FWO), and Friedman (FR). While FR is a differential approach, KAS and FWO are integral approaches. These techniques are most widely used in non-isothermal kinetic studies and have an isoconversional approach.

3.4.1. KAS Method. The integral KAS approach^{62,63} is based on the Coats–Redfern (CR) estimate.⁶⁴ With this method, we use the equation,

$$\ln\left(\frac{\beta}{T^2}\right) = \ln\left(\frac{AR}{E_a f(\alpha)}\right) - \frac{E_a}{RT} \quad (7)$$

In this equation, β , E_a , A , T , $f(\alpha)$, and R represent heating rate, activation energy, phonon frequency factor, absolute temperature at which DTG peaks occur, integral transform function, and universal gas constant, respectively.

The graph of $\ln(\beta/T^2)$ vs $1/T$ is plotted for a fixed value of α , which yields a straight line. The straight line has a slope and intercept of $-(E_a/R)$ and $\ln(AR/E_a f(\alpha))$, respectively. The slope and intercept are useful in determining kinetic parameters like activation energy (E_a) and phonon frequency factor (A):

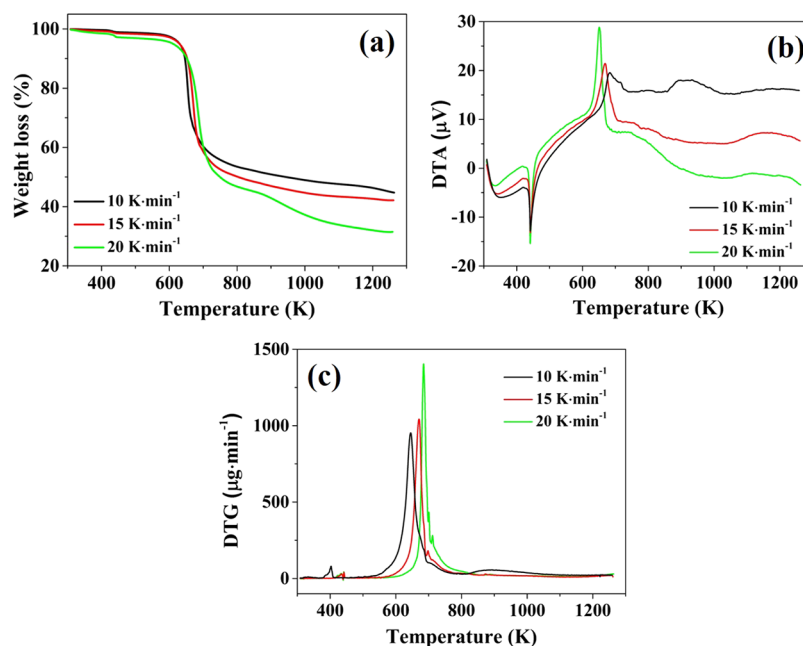


Figure 8. (a) TG, (b) DTA, and (c) DTG thermocurves of the sample.

Table 2. Temperature Range and Observed Weight Loss of the Sample

temperature range (K)	
308–1263	
heating rate (K·min ⁻¹)	weight loss (%)
10	55.27
15	57.85
20	68.51

$$E_a = -(\text{slope} \cdot R) \quad (8)$$

$$A = \frac{E_a \cdot \exp(\text{intercept})}{R} \quad (9)$$

Figure 9 exhibits the KAS plot of the sample having a single decomposition peak.

3.4.2. FWO Method. The equation below is the basis for the integral FWO approach:^{65,66}

$$\ln \beta = -1.052 \left(\frac{E_a}{RT} \right) + \ln \left(\frac{AE_a}{R} \right) - \ln(f(\alpha)) - 5.33 \quad (10)$$

The meaning of each term in this equation is the same as it is in the KAS approach.

Plotting $\ln \alpha$ vs $1/T$ will provide a straight line with a fixed value of α . The straight line has a slope and intercept of $-1.052(E_a/R)$ and $\ln(AE_a/R)$, respectively. The slope and intercept are useful in determining kinetic parameters like activation energy (E_a) and phonon frequency factor (A):

$$E_a = - \left(\frac{\text{slope} \cdot R}{1.052} \right) \quad (11)$$

$$A = \frac{R \cdot \exp(\text{intercept})}{E_a} \quad (12)$$

Figure 10 exhibits the FWO plot of the sample having a single decomposition peak.

3.4.3. FR Method. The equation below is the basis for the differential FR approach⁶⁷

$$\ln \left(\beta \frac{d\alpha}{dt} \right) = \ln(A \cdot f(\alpha)) - \frac{E_a}{RT} \quad (13)$$

$d\alpha/dt$ refers to the differential rate of change of the degree of decomposition in this context. With a fixed value of α , a

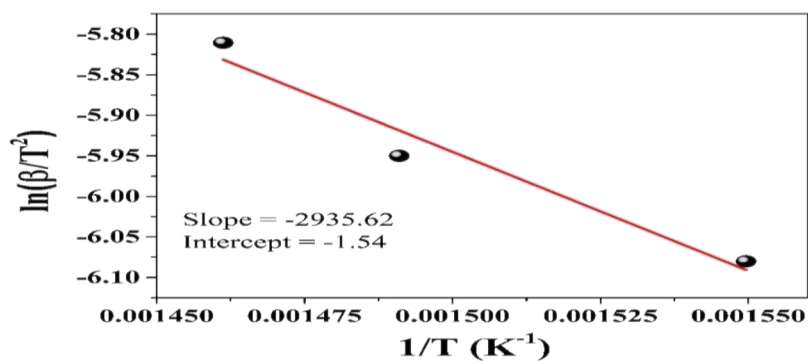


Figure 9. KAS plot.

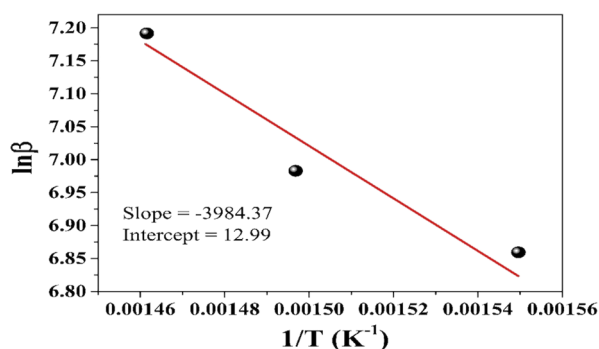


Figure 10. FWO plot.

straight line may be found in a plot of $\ln(\beta \cdot d\alpha/dt)$ vs $1/T$. The fitted line has a slope and intercept of $-(E_a/R)$ and $\ln(A \cdot f(\alpha))$, respectively. Determining kinetic parameters like the activation energy (E_a) and phonon frequency factor (A) with the help of the slope and intercept,

$$E_a = -(\text{slope} \cdot R) \quad (14)$$

$$A = \frac{\exp(\text{intercept})}{f(\alpha)} \quad (15)$$

Figure 11 exhibits the FR plot of the sample having a single decomposition peak.

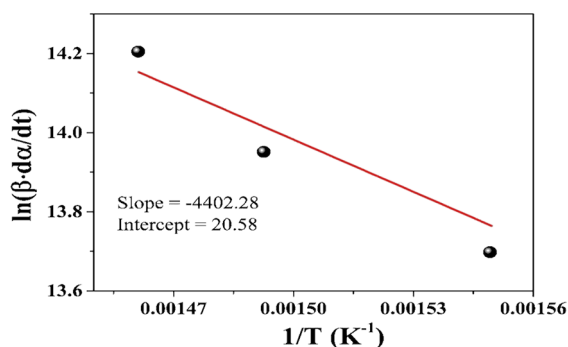


Figure 11. FR plot.

Based on the estimated E_a and A values using KAS, FWO, and FR techniques, the following equations are used to compute the change in activation enthalpy (ΔH^*), entropy (ΔS^*), and Gibb's free energy (ΔG^*):

$$\Delta H^* = E_a - RT \quad (16)$$

$$\Delta S^* R \cdot \ln\left(\frac{Ah}{k_B T}\right) \quad (17)$$

$$\Delta G^* = \Delta H^* - T\Delta S^* \quad (18)$$

Table 3 displays the predicted values for E_a , A , ΔH^* , ΔS^* , and ΔG^* .

The computed kinetic parameters from the three methods are presented in Table 3. This finding demonstrates the validity of the predictions given by the three thermal approaches.

The positive ΔH^* values demonstrate that heat absorption causes decomposition. Negative values of ΔS^* represent an increase in disorder. The positive ΔG^* values indicate that the decomposition is non-spontaneous. This is attributed to

Table 3. Kinetic Parameters

method	E_a (kJ·mol ⁻¹)	A (s ⁻¹)	ΔH^* (kJ·mol ⁻¹)	ΔS^* (J·K ⁻¹ ·mol ⁻¹)	ΔG^* (kJ·mol ⁻¹)
KAS	24.41	628.35	18.86	-198.06	150.92
FWO	31.49	116.46	25.95	-212.08	167.36
FR	36.60	23.79	31.05	-225.29	181.27

decomposition caused by a slow and continuous increase in temperature.

3.5. Biological Activities. **3.5.1. Anti-Inflammatory (Inhibition of Albumin Denaturation) Activity of the Synthesized Compound.** When subjected to an external stressor or substance, such as a potent acid or base, a concentrated inorganic salt, an organic solvent, or heat, proteins can lose both their secondary and tertiary structures.⁶⁸ Most biological proteins become denatured and cease to function biologically. Protein denaturation is known to increase inflammation. The potential of Schiff base to prevent protein denaturation was investigated as part of the investigation into the mechanism of the anti-inflammation action. It worked well to lessen the denaturation of albumin brought on by heat.

Anusuya et al.⁶⁹ described a 2-hydroxy benzoic acid (3-hydroxy benzylidene)-hydrazide-based Schiff base derivative, which was synthesized and evaluated for its anti-inflammatory activity by albumin denaturation and compared with standard aspirin. For the 2-hydroxy benzoic acid (3-hydroxy benzylidene)-hydrazide, the result shows that the percentage of protein denaturation at 500 $\mu\text{g/mL}$ was found to be 60%, while the Schiff base derivative synthesized here in this research article showed 65.33% of protein denaturation at 500 $\mu\text{g/mL}$. Aspirin, a common anti-inflammatory medication, demonstrated the greatest inhibition of 80% at a concentration of 500 $\mu\text{g/mL}$ as shown in Table 4.

Table 4. Anti-Inflammatory Activity of the Schiff Base by the Albumin Denaturation Test

concentration ($\mu\text{g/mL}$)	% of protein denaturation	
	aspirin (standard)	Schiff base
100	42.7	28.0
200	53.3	38.7
300	61.3	46.7
400	69.3	56.0
500	80.00	65.33

3.5.2. Antidiabetic Activity Using α -Amylase Inhibition Assay. The antidiabetic efficacy of the synthesized compound was primarily assessed using α -amylase inhibition, and the result was contrasted with those of standard acarbose (80.80% inhibition). Anusuya et al.⁶⁹ described the antidiabetic activity of a 2-hydroxy benzoic acid (3-hydroxy benzylidene)-hydrazide-based Schiff base derivative by α -amylase inhibition assay and compared with standard acarbose; the result showed 59% α -amylase inhibition, while the Schiff base derivative here in this research article showed 81.09% α -amylase inhibition. Moreover, we also conducted a molecular docking study for the synthesized Schiff base for pancreatic α -amylase, and as a result, the binding energy found for the synthesized compound in current work was found to be -9.4 kcal/mol, while for the standard acarbose, it was -7.5 kcal/mol.

As shown in Table 5, the Schiff base that was developed synthetically displayed better α -amylase inhibition than

Table 5. α -Amylase Inhibition of the Schiff Base and Standard Acarbose

compound name	% α -amylase inhibition
Schiff base	81.09
acarbose standard	80.80

standard acarbose. The highest level of α -amylase inhibition, 81.09%, was found in the Schiff base. The synergy of all the structural components of the Schiff base compound, in particular the imine functionality and phenyl ring with various substituents, is reasonable for its inhibitory potentials. The basic structural components that are present in the structure of the synthesized molecule are the phenyl rings and the imine functionality.

3.6. Molecular Docking Study. The binding orientation of the Schiff base to pancreatic α -amylase was predicted using molecular docking experiments, which were also utilized to investigate the specific intermolecular interactions. Using the Schiff base and standard acarbose, the wild form of human pancreatic α -amylase (PDB ID: 4X9Y) was docked. The docking scores (binding energy) are shown in Table 6. It is

Table 6. Binding Energy of Schiff Bases and Standard Acarbose

compound name	binding energy (kcal/mol)
Schiff base	-9.4
acarbose standard	-7.5

significant to note that the Schiff base exhibited a good binding energy of -9.4 kcal/mol compared to the typical amylase inhibitor acarbose (-7.50 kcal/mol). The binding mechanisms of Schiff base and acarbose to receptors were examined using Discovery Studio 4.5. Schiff base and acarbose interactions with the active region (4X9Y) of the receptor are depicted in 2D representations as shown in Figure 12a,b.

3.6.1. In Silico Analysis. The biological activities of the Schiff base were identified using *in silico* analysis. According to an examination of its anticipated biological activities, the developed compound showed a >27% ($P_a > 0.3$) possibility of displaying 133 biological activities. There are 69 activities with a high chance of occurring ($P_a > 0.7$), whereas 22 have a moderate chance of occurring ($P_a > 0.5$). Antimicrobial activities made up 11 of the total activity found (Table 7). It was possible to determine oral bioavailability and anticipate toxicity. Using the synthesized compound's TPSA, iLogP, molecular weight, nALH, and nDLH values, oral bioavailability was estimated. The Schiff base compound has a high estimated oral bioavailability (TPSA = 24.72; LogP = 7.62; molecular weight of 457.39 g/mol) since it fits the criteria. With a molecular weight of 331.34 g/mol, ciprofloxacin displayed a TPSA of 74.57, 2.24 iLogP, 2.0 nDLH, and 5.0 nALH.

3.6.2. Prediction of ADMET Properties. According to *in silico* ADMET analysis, the bioactivity and low toxicity of molecules are given preference for the discovery of drugs and their further developments. *In silico* screening of ADMET characteristics based on the molecular structure is a highly effective method for identifying drug candidates. Early prediction of ADMET features in the drug development

process reduces the failure rate of pharmacokinetic parameters during clinical stages, enhancing discovery phase efficiency. The ADMET parameters of the Schiff base are shown in Table 8.

The Schiff base is closely associated with the absorption characteristics of chemicals. The TPSA of the Schiff base was 24.72, indicating that the compounds were non-polar and readily absorbed by the body. The Schiff base has low solubility, high permeability, moderate-to-high metabolism, and substantial oral absorption or membrane permeability. It was expected to have excellent lipophilicity (AlogP98_5). The synthesized molecule was shown to have poor absorption and permeability throughout this experiment. The amount of drug absorption was predicted using Caco-2 permeability values, human stomach absorption, permeability via the skin, and either inhibition or substrate usage of P-glycoprotein. The anticipated result is -4.76 cm/s when the Papp coefficient is greater than -4.7; hence, the chemical has an enhanced Caco-2 permeability and hence can be easily absorbed. Anything that absorbs more than 30% of its weight in the human gut is termed well absorbed. The synthesized compound was expected to be adequately absorbed by the human gut. The compound has a log Kp > -3.32 (cm/s) in terms of skin permeability and is assumed to have mild skin permeability. An adenosine triphosphate (ATP)-binding transmembrane protein known as the ATP-binding cassette (ABC) is the glycoprotein that removes medicine and other foreign compounds from cells. The results showed that the synthesized molecules were not P-glycoprotein substrates and that P-glycoprotein did not actively remove them from cells. It was predicted that the synthesized compound would not inhibit P-glycoprotein. Drug distribution was described using volume distribution (VDss), percent unbound in humans, permeability in the central nervous system, and blood-brain barrier bridging (logBB). The distribution volume is a measurement used to assess how medications are dispersed among an organism's various tissues. A VDss of less than 0.71 L/kg reveals the volume (log VDss = 0.15). P-glycoprotein non-inhibitors were expected to be the produced molecule. Drug distribution was described using volume distribution (VDss), human percent unbound, central nervous system (CNS) permeability, and blood-brain barrier crossing (logBB). An indicator of how medications are spread among an organism's many tissues is the distribution volume. The volume is indicated by a less-than 0.71 L/kg VDss (log VDss = 0.15). The blood-brain barrier was supposed to be difficult for the created substance to cross. When VDss is more than 2.81 L/kg (log VDss > 0.45), the distribution volume is considered to be fairly large. According to the findings, the synthesized molecule's distribution volume was small and its VDss was 0.403 L/kg. The blood-brain barrier membrane was expected to let the compounds cross with a logBB > 0.3 permeability. A logBB-1 revealed that the medication had difficulty crossing the blood-brain barrier. The chemical was expected to have difficulty passing the blood-brain barrier. The anticipated results show that the compound's high lipophilicity caused the ADMET properties to be quickly digested and eliminated. It readily passes the blood-brain barrier and is devoid of AMSE. The selection of a molecule that may eventually be prescribed as an oral medication with high bioavailability can be aided by the prediction of drug similarity variables. We used the recommendations from Lipinski, Ghose, Veber, Egan, and Muegge to investigate the indicated compounds' oral

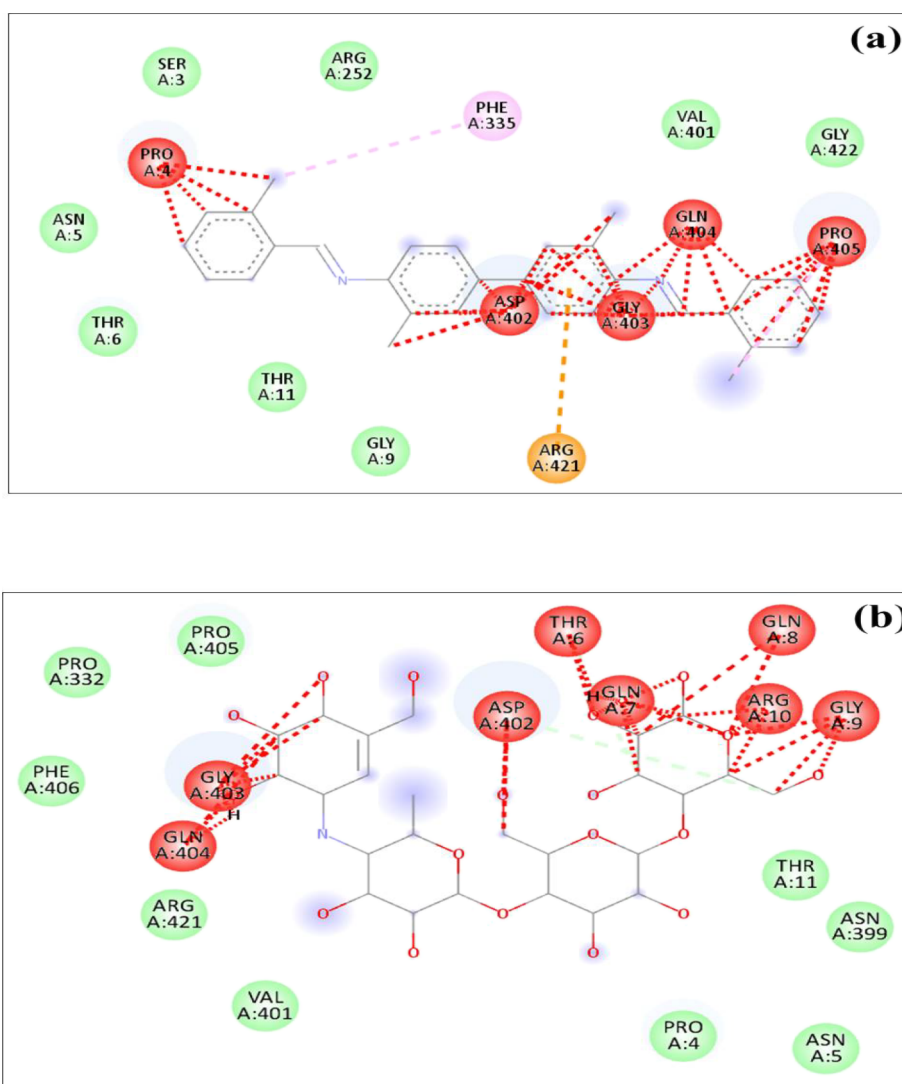


Figure 12. (a) Interaction of the Schiff base with 4X9Y and (b) interaction of standard acarbose with 4X9Y.

Table 7. *In Silico* Identification of the Activities

activity	Pa value	Pi value
IgA-specific serine end peptidase inhibitor	0.745	0.01
phobic disorders treatment	0.681	0.085
insulysin inhibitor	0.623	0.02
muscular dystrophy treatment	0.515	0.015
gastrin inhibitor	0.489	0.074
membrane permeability inhibitor	0.422	0.193
antiparasitic	0.41	0.029
antiprotozoal (leishmania)	0.402	0.048
vasoprotector	0.382	0.087
erythropoietin stimulant	0.376	0.106
antiprotozoal (coccidial)	0.372	0.028
antituberculosic	0.369	0.042
insecticide	0.363	0.009
antibacterial	0.49	0.055
antiviral (picornavirus)	0.349	0.16
antihypoxic	0.341	0.12
antineurotic	0.327	0.221
urticaria treatment	0.314	0.009
dementia treatment	0.309	0.131

bioavailability and drug-likeness. With a few exceptions, it has largely adhered to the five guidelines. Table 8 depicts the features of the synthesized Schiff base in terms of their pharmacological similarities. As compared to the reference molecule ciprofloxacin, the compound had notable physicochemical, pharmacokinetic, and drug-like features.

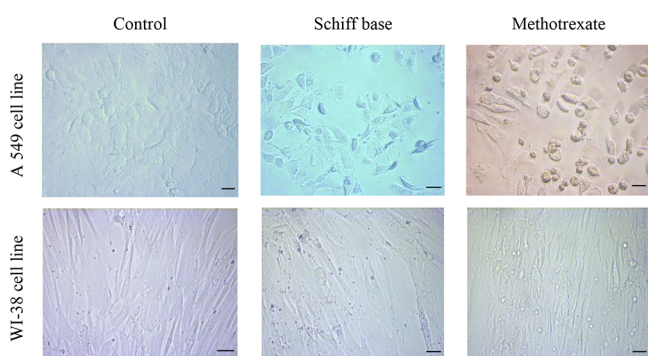
3.7. *In Vitro* Cytotoxicity Study. The concentration of Schiff base compound that, after 24 h of treatment, results in a 50% viability inhibition for the A549 cell line is shaded in the findings obtained (Figure 13). The obtained results indicate that the Schiff base exhibited an IC_{50} value of 288.2 ± 0.378 $\mu\text{g/mL}$ against A549 cells, while it showed an IC_{50} value of 490.50 ± 0.590 $\mu\text{g/mL}$ against WI-38 cells. In comparison, the standard drug methotrexate demonstrated IC_{50} values of 10.20 ± 1.82 $\mu\text{g/mL}$ on A549 cells and 26.21 ± 1.14 $\mu\text{g/mL}$ on WI-38 cells. These findings provide evidence that the Schiff base is highly effective in terms of cytotoxicity against A549 cells while exhibiting lower toxicity toward normal lung epithelial cells (WI-38).

4. CONCLUSIONS

The synthesis and spectral characterization of Schiff base derived from 2-chloro benzaldehyde and 3,3'-dimethyl-[1,1'-

Table 8. Predicted ADMET Properties of a Compound

property	Schiff base	ciprofloxacin
TPSA	24.72	74.57
LogS (solubility)	-7.303	-3.285
LogD7.4 (distribution coefficient D)	3.533	-0.705
LogP (distribution coefficient P)	8.768	1.583
Absorption		
water solubility (log mol/L)	-7.303	-3.285
Caco-2 permeability (log Papp in 10 ⁻⁶ cm/s)	-4.763	-5.165
P-glycoprotein-inhibitor	no	no
P-glycoprotein-substrate	yes	yes
HIA (human intestinal absorption)	yes	yes
Distribution		
PPB (plasma protein binding)	84.787	69.358
BBB (blood–brain barrier)	no	no
VD (volume distribution) (human, log L/kg)	0.403	0.503
Metabolism		
P450 CYP1A2 inhibitor	no	no
P450 CYP1A2 substrate	yes	yes
CYP450 3A4 inhibitor	no	no
CYP450 3A4 substrate	yes	no
CYP450 2C9 inhibitor	no	no
CYP450 2C9 substrate	yes	no
CYP450 2C19 inhibitor	no	no
CYP450 2C19 substrate	yes	no
CYP450 2D6 inhibitor	no	no
CYP450 2D6 substrate	yes	no
Excretion		
total clearance (log mL/min/kg)	0.829	1.316
T _{1/2} (half-life time)	2.287	1.857
Toxicity		
hERG (hERG blockers)	yes	no
H-HT (human hepatotoxicity)	no	yes
8AMES (Ames mutagenicity)	no	yes
SkinSen (skin sensitization)	yes	no

**Figure 13.** Morphological changes induced by Schiff base and methotrexate standard drug on A549 and WI-38 cells. The scale bar represents the average size of cells (12 μm).

biphenyl]-4,4'-diamine are accomplished. The results obtained from the XRD outcome revealed that the sample possesses a triclinic structure having lattice parameters $a = 9.56 \text{ \AA}$, $b = 9.65 \text{ \AA}$, $c = 14.76 \text{ \AA}$, $\alpha = 88.82^\circ$, $\beta = 86.82^\circ$, and $\gamma = 76.12^\circ$. Using Scherrer's formula, the estimated crystallite size from the XRD data is 21.40 nm. The dislocation density is found to be $2.18 \times 10^{15} \text{ m}^{-2}$. The existence of $\nu(\text{C}=\text{N})$ is demonstrated by the FTIR, $^1\text{H-NMR}$, and $^{13}\text{C-NMR}$. The molecular ion peak in the MS spectrum is at $m/z = 458$, which is in good agreement with the molecular weight of the substance (457). In an atmosphere

of inert nitrogen, TG thermocurves were obtained from a range of temperatures between 308 and 1263 K at three distinct heating rates (10, 15, and 20 $\text{K}\cdot\text{min}^{-1}$). Due to the loss of hydrate samples, DTA thermocurves initially exhibited endothermic activity, and as the sample broke down, exothermic behavior was seen. The KAS, FWO, and FR techniques are used to estimate the kinetic parameters. The three strategies' correctness is demonstrated by the good agreement between the estimated parameters utilizing each method. The synthesized Schiff base has a moderate anti-inflammatory effect according to an *in vitro* assessment of albumin denaturation bioassay. In the research on antidiabetic properties of this substance, the inhibition of α -amylase enzymes may contribute to reducing postprandial glucose levels in the blood. This mechanism plays a crucial role in the effective control of blood sugar. The synthesized compound, developed with ADMET (Absorption, Distribution, Metabolism, Excretion, and Toxicity) in mind, has the potential to recommend a promising candidate for future drug research. The Schiff base has good oral bioavailability and pharmacological similarity per the five criteria, and the results are reasonable. While drugs are readily digested in the gastrointestinal (GI) tract, the blood–brain barrier (BBB) acts as a barrier preventing their passage into the brain. The lead compound exhibits favorable pharmacokinetic characteristics, as it does not raise any concerns according to PAINS (Pan Assay Interference Compounds) warnings, unlike the reference medication.

■ AUTHOR INFORMATION

Corresponding Author

Jatin D. Patel – Department of Chemistry, Shri Alpesh N. Patel Post Graduate Institute of Science and Research, Anand 388001 Gujarat, India; orcid.org/0000-0001-8311-9522; Phone: +91 98253 55242; Email: jdpatel_pri@sanppgi.ac.in

Authors

Priteshkumar M. Thakor – Department of Chemistry, Shri Alpesh N. Patel Post Graduate Institute of Science and Research, Anand 388001 Gujarat, India; orcid.org/0000-0002-6121-2168

Rajesh J. Patel – Department of Chemistry, Shri Alpesh N. Patel Post Graduate Institute of Science and Research, Anand 388001 Gujarat, India

Ranjan Kr. Giri – P. G. Department of Physics, Sardar Patel University, Vallabh Vidyanagar 388120 Gujarat, India; orcid.org/0000-0002-9702-1566

Sunil H. Chaki – P. G. Department of Physics, Sardar Patel University, Vallabh Vidyanagar 388120 Gujarat, India

Ankurkumar J. Khimani – Department of Physics, Shri Alpesh N. Patel Post Graduate Institute of Science and Research, Anand 388001 Gujarat, India

Yati H. Vaidya – Department of Microbiology, Shri Alpesh N. Patel Post Graduate Institute of Science and Research, Anand 388001 Gujarat, India

Parth Thakor – B. D. Patel Institute of Paramedical Sciences, Charotar University of Science and Technology, Changa 388421 Gujarat, India; orcid.org/0000-0002-7477-0177

Anjali B. Thakkar – P. G. Department of Biosciences and P. G. Department of Applied and Interdisciplinary Sciences, Sardar Patel University, Anand 388120 Gujarat, India

Complete contact information is available at:

<https://pubs.acs.org/10.1021/acsomega.3c05254>

Notes

The authors declare no competing financial interest. The work does not include any statements that are offensive or illegal, violate anybody else's rights, or contain any information that could lead to harm or injury. No data is associated with the manuscript.

REFERENCES

- (1) Katouah, H.; Hameed, A. M.; Alharbi, A.; Alkhatib, F.; Shah, R.; Alzahrani, S.; Zaky, R.; El-Metwaly, N. M. Green Synthesis Strategy for New Schiff-Base Complexes: Characterization, Conductometry, *In Vitro* Assay Confirmed by *In Silico* Approach. *ChemistrySelect* **2020**, *5*, 10256–10268.
- (2) Boruah, J. J.; Bhatt, Z. S.; Nathani, C. R.; Bambhaniya, V. J.; Guha, A. K.; Das, S. P. Green Synthesis of a Vanadium(V) Schiff Base Complex by Grinding Method: Study on Its Catalytic and Antibacterial Activity. *J. Coord. Chem.* **2021**, *74*, 2055–2068.
- (3) Hassan, A. M.; Said, A. O.; Heikal, B. H.; Younis, A.; Aboalthana, W. M.; Mady, M. F. Green Synthesis, Characterization, Antimicrobial and Anticancer Screening of New Metal Complexes Incorporating Schiff Base. *ACS Omega* **2022**, *7*, 32418–32431.
- (4) Shebl, M. Mononuclear, Homo- and Hetero-Binuclear Complexes of 1-(5-(1-(2-Aminophenylimino)Ethyl)-2,4-Dihydroxyphenyl)Ethanone: Synthesis, Magnetic, Spectral, Antimicrobial, Antioxidant, and Antitumor Studies. *J. Coord. Chem.* **2016**, *69*, 199–214.
- (5) Woźniczka, M.; Świątek, M.; Sutradhar, M.; Gądek-Sobczyńska, J.; Chmiela, M.; Gonciarz, W.; Pasternak, B.; Pająk, M. Equilibria of Complexes in the Aqueous Cobalt(II)–N-(2-Hydroxybenzyl)-Phenylalanine System and Their Biological Activity Compared to Analogous Schiff Base Structures. *Comput. Struct. Biotechnol. J.* **2023**, *21*, 1312–1323.
- (6) El-Shwiniy, W. H.; Ibrahim, A. G.; Sadeek, S. A.; Zordok, W. A. Synthesis, Structural Elucidation, Molecular Modeling and Antimicrobial Studies of 6-(2-Hydroxyphenylimine)-2-Thioxotetrahydropyrimidin-4(1H)-One (L) Schiff Base Metal Complexes. *Appl. Organomet. Chem.* **2021**, *35*, No. e6174.
- (7) El-Attar, M. S.; Ahmed, F. M.; Sadeek, S. A.; Mohamed, S. F.; Zordok, W. A.; El-Shwiniy, W. H. Characterization, DFT, and Antimicrobial Evaluation of Some New N2O2 Tetradentate Schiff Base Metal Complexes. *Appl. Organomet. Chem.* **2022**, *36*, No. e6826.
- (8) Haj, N. Q.; Mohammed, M. O.; Mohammed, L. E. Synthesis and Biological Evaluation of Three New Chitosan Schiff Base Derivatives. *ACS Omega* **2020**, *5*, 13948–13954.
- (9) Nyawade, E. A.; Onani, M. O.; Meyer, S.; Dube, P. Synthesis, Characterization and Antibacterial Activity Studies of New 2-Pyrral-L-Amino Acid Schiff Base Palladium (II) Complexes. *Chem. Pap.* **2020**, *74*, 3705–3715.
- (10) Hejchman, E.; Kruszewska, H.; Maciejewska, D.; Sowirka-Taciak, B.; Tomczyk, M.; Sztokfisz-Ignasiak, A.; Jankowski, J.; Młynarczuk-Biały, I. Design, Synthesis, and Biological Activity of Schiff Bases Bearing Salicyl and 7-Hydroxycoumarinyl Moieties. *Monatshefte für Chemie* **2019**, *150*, 255–266.
- (11) Sharma, B. P.; Adhikari Subin, J.; Marasini, B. P.; Adhikari, R.; Pandey, S. K.; Sharma, M. L. Triazole Based Schiff Bases and Their Oxovanadium(IV) Complexes: Synthesis, Characterization, Antibacterial Assay, and Computational Assessments. *Heliyon* **2023**, *9*, No. e15239.
- (12) Afzal, H. R.; Khan, N. U. H.; Sultana, K.; Mobashar, A.; Lareb, A.; Khan, A.; Gull, A.; Afzaal, H.; Khan, M. T.; Rizwan, M.; Imran, M. Schiff Bases of Pioglitazone Provide Better Antidiabetic and Potent Antioxidant Effect in a Streptozotocin-Nicotinamide-Induced Diabetic Rodent Model. *ACS Omega* **2021**, *6*, 4470–4479.
- (13) Szklarzewicz, J.; Jurowska, A.; Hodorowicz, M.; Kazek, G.; Mordyl, B.; Menaszek, E.; Sapa, J. Characterization and Antidiabetic Activity of Salicylhydrazone Schiff Base Vanadium(IV) and (V) Complexes. *Transition Met. Chem.* **2021**, *46*, 201–217.
- (14) Sinicropi, M. S.; Ceramella, J.; Iacopetta, D.; Catalano, A.; Mariconda, A.; Rosano, C.; Saturnino, C.; El-Kashef, H.; Longo, P. Metal Complexes with Schiff Bases: Data Collection and Recent Studies on Biological Activities. *Int. J. Mol. Sci.* **2022**, *23*, 14840.
- (15) Omer, A. M.; Eltaweil, A. S.; El-Fakharany, E. M.; Abd El-Monaem, E. M.; Ismail, M. M. F.; Mohy-Eldin, M. S.; Ayoub, M. S. Novel Cytocompatible Chitosan Schiff Base Derivative as a Potent Antibacterial, Antidiabetic, and Anticancer Agent. *Arab. J. Sci. Eng.* **2023**, *48*, 7587–7601.
- (16) Aroua, L. M.; Al-Hakimi, A. N.; Abdulghani, M. A. M.; Alhag, S. K. Cytotoxic Urea Schiff Base Complexes for Multidrug Discovery as Anticancer Activity and Low *In Vivo* Oral Assessing Toxicity. *Arab. J. Chem.* **2022**, *15*, No. 103986.
- (17) Manjare, S. B.; Mahadik, R. K.; Manval, K. S.; More, P. P.; Dalvi, S. S. Microwave-Assisted Rapid and Green Synthesis of Schiff Bases Using Cashew Shell Extract as a Natural Acid Catalyst. *ACS Omega* **2023**, *8*, 473.
- (18) Packialakshmi, P.; Gobinath, P.; Ali, D.; Alarifi, S.; Gurusamy, R.; Idhayadhulla, A.; Surendrakumar, R. New Chitosan Polymer Scaffold Schiff Bases as Potential Cytotoxic Activity: Synthesis, Molecular Docking, and Physicochemical Characterization. *Front. Chem.* **2022**, *9*, 1–12.
- (19) Abood, H. S.; Ramadhan, U. H.; Hamza, H. Synthesis and Anti-Inflammatory Activity Study of Schiff Bases Complexes. *Biochem. Cell. Arch.* **2020**, *20*, 5627–5631.
- (20) Obaleye, J. A.; Aliyu, A. A.; Rajee, A. O.; Bello, K. E. Synthesis, Characterization, *In-Vitro* Anti-Inflammatory and Antimicrobial Screening of Metal(Ii) Mixed Diclofenac and Acetaminophen Complexes. *Bull. Chem. Soc. Ethiop.* **2021**, *35*, 77–86.
- (21) Hamid, S. J.; Salih, T. Design, Synthesis, and Anti-Inflammatory Activity of Some Coumarin Schiff Base Derivatives: *In Silico* and *In Vitro* Study. *Drug Des. Devel. Ther.* **2022**, *Volume 16*, 2275–2288.
- (22) Shi, J.; Zhou, Y.; Wang, K.; Ma, Q.; Wei, R.; Li, Q.; Zhao, Y.; Qiao, Z.; Liu, S.; Leng, Y.; Liu, W.; Sang, Z. Design, Synthesis and Biological Evaluation of Schiff's Base Derivatives as Multifunctional Agents for the Treatment of Alzheimer's Disease. *Med. Chem. Res.* **2021**, *30*, 624–634.
- (23) Patchipala, S. B.; Pasupuleti, V. R.; Audipudi, A. V.; Bollikolla, H. b. Synthesis, *In-Vivo* Anti-Diabetic & Anticancer Activities and Molecular Modelling Studies of Tetrahydrobenzo[d]Thiazole Tethered Nicotinohydrazide Derivatives. *Arab. J. Chem.* **2022**, *15*, No. 103546.
- (24) Gulati, S.; Singh, R.; Sindhu, J.; Sangwan, S. Eco-Friendly Preparations of Heterocycles Using Fruit Juices as Catalysts: A Review. *Org. Prep. Proced. Int.* **2020**, *52*, 381–395.
- (25) Soliman, A. I. A.; Sayed, M.; Elshahawany, M. M.; Younis, O.; Ahmed, M.; Kamal El-Dean, A. M.; Abdel-Wahab, A. M. A.; Wachtveitl, J.; Braun, M.; Fatehi, P.; Tolba, M. S. Base-Free Synthesis and Photophysical Properties of New Schiff Bases Containing Indole Moiety. *ACS Omega* **2022**, *7*, 10178–10186.
- (26) Ma'rufah, L.; Hanapi, A.; Ningsih, R.; Fasya, A. G. Synthesis of Schiff Base Compounds from Vanillin and p -Aminoacetophenone Using Lime Juice as a Natural Acid Catalyst and Their Utilization as Corrosion Inhibitors. *Proc. Int. Conf. Eng. Technol. Soc. Sci. (ICONETOS 2020)* **2021**, *529*, 297–301.
- (27) Anila Raj, S.; Vidya, V. G.; Preethi, V.; Viju Kumar, V. G. Single Crystal XRD and DFT Investigation of 1,5-Dimethyl-4-[(2-Oxo-1,2-Diphenylethylidene) Amino]-2-Phenyl-1,2-Dihydro-3H-Pyrazol-3-One. *Results Chem.* **2022**, *4*, No. 100665.
- (28) Adly, O. M. I.; Shebl, M.; Abdelrhman, E. M.; El-Shetary, B. A. Synthesis, Spectroscopic, X-Ray Diffraction, Antimicrobial and Antitumor Studies of Ni(II) and Co(II) Complexes Derived from 4-Acetyl-5,6-Diphenyl-3(2H)-Pyridazinone and Ethylenediamine. *J. Mol. Struct.* **2020**, *1219*, No. 128607.
- (29) Radha, V. P.; Prabakaran, M. Novel Thiadiazole-Derived Schiff Base Ligand and Its Transition Metal Complexes: Thermal Behaviour,

Theoretical Study, Chemo-Sensor, Antimicrobial, Antidiabetic and Anticancer Activity. *Appl. Organomet. Chem.* **2022**, *36*, No. e6872.

(30) Qidwai, T. QSAR Modeling, Docking and ADMET Studies for Exploration of Potential Anti-Malarial Compounds against Plasmodium Falciparum. *silico Pharmacol.* **2017**, *5*, 1–13.

(31) Subin Kumar, K. Design, One-Pot Synthesis, Cytotoxic, in Vivo Anticancer, Antioxidant and Antimicrobial Evaluation of a Novel Mixed Schiff Base Ligand and Its Metal Complexes. *Results Chem.* **2022**, *4*, No. 100463.

(32) Uddin, N.; Rashid, F.; Ali, S.; Tirmizi, S. A.; Ahmad, I.; Zaib, S.; Zubair, M.; Diaconescu, P. L.; Tahir, M. N.; Iqbal, J.; Haider, A. Synthesis, Characterization, and Anticancer Activity of Schiff Bases. *J. Biomol. Struct. Dyn.* **2020**, *38*, 3246–3259.

(33) Patel, J. D. Natural Acid-Catalyzed Synthesis Of 6,6'-(((3,3'-Dimethoxy-[1,1'-Biphenyl]-4,4'-Diyl) bis (azanylylidene)) bis (methanylylidene)) bis (2 , 4-dichlorophenol), its conventionally synthesized metal complexes and their potential as biological agents. **2023**, *16* (), 61–68.

(34) Uwaya, D.; Okakwu, R.; Omozuwa, O. In-Vivo and In-Vitro Anti-Inflammatory Activities of the Aqueous Extract of Di-Herbal Formulation (Euphorbia Hirta and Lactuca Virosa). *J. Appl. Sci. Environ. Manag.* **2021**, *24*, 1979–1985.

(35) Naz, R.; Ayub, H.; Nawaz, S.; Islam, Z. U.; Yasmin, T.; Bano, A.; Wakeel, A.; Zia, S.; Roberts, T. H. Antimicrobial Activity, Toxicity and Anti-Inflammatory Potential of Methanolic Extracts of Four Ethnomedicinal Plant Species from Punjab, Pakistan. *BMC Complement. Altern. Med.* **2017**, *17*, 1–13.

(36) Obaseki, O. E.; Adesegun, O. I.; Anyasor, G. N.; Abebawo, O. O. Evaluation of the Anti-Inflammatory Properties of the Hexane Extract of Hydrocotyle Bonariensis Comm. Ex Lam. Leaves. *Afr. J. Biotechnol.* **2016**, *15*, 2759–2771.

(37) Bernfield, P. Amylase, Alpha and Beta. *Methods Enzym.* **1955**, *1*, 149–158.

(38) Lankisch, M.; Layer, P.; Rizza, R. A.; DiMugno, E. P. Acute Postprandial Gastrointestinal and Metabolic Effects of Wheat Amylase Inhibitor (WAI) in Normal, Obese, and Diabetic Humans. *Pancreas* **1998**, *17*, 176–181.

(39) Roux, M. J.; Martínez-Maza, R.; Le Goff, A.; López-Corcuera, B.; Aragón, C.; Supplisson, S. The Glial and the Neuronal Glycine Transporters Differ in Their Reactivity to Sulfhydryl Reagents. *J. Biol. Chem.* **2001**, *276*, 17699–17705.

(40) Allouche, A. Gabedit — A Graphical User Interface for Computational Chemistry Softwares. *J. Comput. Chem.* **2011**, *32*, 174–182.

(41) Singhal, S.; Khanna, P.; Khanna, L. Synthesis, DFT Studies, Molecular Docking, Antimicrobial Screening and UV Fluorescence Studies on Ct-DNA for Novel Schiff Bases of 2-(1-Aminobenzyl) Benzimidazole. *Heliyon* **2019**, *5*, No. e02596.

(42) Namera, D. L.; Thakkar, S. S.; Thakor, P.; Bhoya, U.; Shah, A. Arylidene Analogues as Selective COX-2 Inhibitors: Synthesis, Characterization, in Silico and in Vitro Studies. *J. Biomol. Struct. Dyn.* **2021**, *39*, 7150–7159.

(43) Halgren, T. A. MMFF VI. MMFF94s Option for Energy Minimization Studies. *J. Comput. Chem.* **1999**, *20*, 720–729.

(44) Fonteh, P.; Elkhadir, A.; Omondi, B.; Guzei, I.; Darkwa, J.; Meyer, D. Impedance Technology Reveals Correlations between Cytotoxicity and Lipophilicity of Mono and Bimetallic Phosphine Complexes. *BioMetals* **2015**, *28*, 653–667.

(45) DeLano, W. L. Pymol: An Open-Source Molecular Graphics Tool. *CCP4 Newsl. Protein Crystallogr* **2002**, *40*, 82–92.

(46) Daina, A.; Michielin, O.; Zoete, V. SwissADME: A Free Web Tool to Evaluate Pharmacokinetics, Drug-Likeness and Medicinal Chemistry Friendliness of Small Molecules. *Sci. Rep.* **2017**, *7*, 1–13.

(47) Khurana, N.; Ishar, M. P. S.; Gajbhiye, A.; Goel, R. K. PASS Assisted Prediction and Pharmacological Evaluation of Novel Nicotinic Analogs for Nootropic Activity in Mice. *Eur. J. Pharmacol.* **2011**, *662*, 22–30.

(48) Deshi, J. J.; Barminas, J. T.; Onwuka, J. C.; Dass, P. M.; Maitera, O. N.; Muazu, I. Antimicrobial Efficacy of Biosynthesized

Silver Nanoparticles from Different Solvent Extracts of Waltheria Americana Root. *J. Anal. Sci. Technol.* **2016**, *7*, 1–9.

(49) Thakor, P.; Subramanian, R. B.; Thakkar, S. S.; Ray, A.; Thakkar, V. R. Phytol Induces ROS Mediated Apoptosis by Induction of Caspase 9 and 3 through Activation of TRAIL, FAS and TNF Receptors and Inhibits Tumor Progression Factor Glucose 6 Phosphate Dehydrogenase in Lung Carcinoma Cell Line (A549). *Biomed. Pharmacother.* **2017**, *92*, 491–500.

(50) Gajera, H. P.; Hirpara, D. G.; Katakpara, Z. A.; Patel, S. V.; Golakiya, B. A. Molecular Evolution and Phylogenetic Analysis of Biocontrol Genes Acquired from SCoT Polymorphism of Mycoparasitic Trichoderma Koningii Inhibiting Phytopathogen Rhizoctonia Solani Kuhn. *Infect. Genet. Evol.* **2016**, *45*, 383–392.

(51) Nassar, A. M.; Hassan, A. M.; Shoeib, M. A.; El kmash, A. N. Synthesis, Characterization and Anticorrosion Studies of New Homobimetallic Co(II), Ni(II), Cu(II), and Zn(II) Schiff Base Complexes. *J. Bio-Tribo-Corros.* **2015**, *1*, 1–16.

(52) Alorini, T. A.; Al-Hakimi, A. N.; El-Sayed Saeed, S.; Alhamzi, E. H. L.; Albadri, A. E. A. E. Synthesis, Characterization, and Anticancer Activity of Some Metal Complexes with a New Schiff Base Ligand. *Arab. J. Chem.* **2022**, *15*, No. 103559.

(53) Asadi, Z.; Asadi, M.; Shorkaei, M. R. Synthesis, Characterization and DFT Study of New Water-Soluble Aluminum(III), Gallium(III) and Indium(III) Schiff Base Complexes: Effect of Metal on the Binding Propensity with Bovine Serum Albumin in Water. *J. Iran. Chem. Soc.* **2016**, *13*, 429–442.

(54) Kadhemi, B. J.; Alshawi, J.; Alsalm, T. A.; Abdalla, M. Novel Schiff Bases Ligands and Their Complexes: Thermal Analysis Antibacterial Activity, and Molecular Docking. *Egypt. J. Chem.* **2022**, *65*, 107–119.

(55) Salehi, M.; Faghani, F.; Kubicki, M.; Bayat, M. New Complexes of Ni(II) and Cu(II) with Tridentate ONO Schiff Base Ligand: Synthesis, Crystal Structures, Electrochemical and Theoretical Investigation. *J. Iran. Chem. Soc.* **2018**, *15*, 2229–2240.

(56) Bartyzel, A. Synthesis, Thermal Behaviour and Some Properties of CuII Complexes with N,O-Donor Schiff Bases. *J. Therm. Anal. Calorim.* **2018**, *131*, 1221–1236.

(57) Patterson, A. L. The Scherrer Formula for X-Ray Particle Size Determination. *Phys. Rev.* **1939**, *56*, 978–982.

(58) Giri, R. K.; Chaki, S.; Khimani, A. J.; Vaidya, Y. H.; Thakor, P.; Thakkar, A. B.; Pandya, S. J.; Deshpande, M. P. Biocompatible CuInS₂Nanoparticles as Potential Antimicrobial, Antioxidant, and Cytotoxic Agents. *ACS Omega* **2021**, *6*, 26533–26544.

(59) Malek, T. J.; Chaki, S. H.; Giri, R. K.; Deshpande, M. P. The Structural, Morphological, and Optical Study of Chemical Bath Deposition and a Spin Coating Deposited Mackinawite FeS Thin Films. *Appl. Phys. A: Mater. Sci. Process.* **2022**, *128*, 830.

(60) Kannaujya, R. M.; Chaki, S. H.; Khimani, A. J.; Parekh, Z. R.; Deshpande, M. P. Kinetic Stability of Tin Telluride Nanoparticles Synthesized by Hydrothermal Method. *Chem. Thermodyn. Therm. Anal.* **2022**, *6*, No. 100058.

(61) Giri, R. K.; Chaki, S. H.; Khimani, A. J.; Patel, S. R.; Deshpande, M. P. Thermal Investigation of Nanospheres and Nanowhiskers of CuInS₂. *Eur. Phys. J. Plus* **2021**, *136*, 320.

(62) Kissinger, H. E. Reaction Kinetics in Differential Thermal Analysis. *Anal. Chem.* **1957**, *29*, 1702–1706.

(63) Akahira, T. Trans. Joint Convention of Four Electrical Institutes. *Res. Rep. Chiba Inst. Technol.* **1971**, *16*, 22–31.

(64) Coats, A. W.; Redfern, J. P. Kinetic Parameters from Thermogravimetric Data. *Nature* **1964**, *201*, 68–69.

(65) Ozawa, T. Estimation of Activation Energy by Isoconversion Methods. *Thermochim. Acta* **1992**, *203*, 159–165.

(66) Abu-Sehly, A. A. Variation of the Activation Energy of Crystallization in Se_{81.5}Te_{16.5}Sb_{2.5} Chalcogenide Glass: Isoconversional Analysis. *Thermochim. Acta* **2009**, *485*, 14–19.

(67) Friedman, H. L. Kinetics of Thermal Degradation of Char-Forming Plastics from Thermogravimetry. Application to a Phenolic Plastic. *J. Polym. Sci. Part C Polym. Symp.* **1964**, *6*, 183–195.

(68) Azam, S.; Ansari, P.; Rashid, M. M. U.; Alam, M. N.; Ahmed, I. H.; Ibarahim, M. Y.; Shafi, S. M.; Rahman, S.; Hossen, A. *In Vitro* Anti-Oxidant and in Vivo Anti-Inflammatory Activity Determination of the Methanolic Leaves Extract of *Millettia pachycarpa*. *Biomed. Res. Ther.* **2015**, *2*, 366–368.

(69) Anusuya, V.; Sujatha, G.; Broheshnu, G. B.; Balaji, G. L. Anti Oxidant, Anti Inflammation and Anti Diabetic Activity of Novel Schiff Base Derived from 2-Hydroxy Benzoic Acid (3-Hydroxy Benzylidene)Hydrazide and 2-Hydroxy Benzoic Acid (3-Hydroxy - 4-Methoxy Benzylidene)-Hydrazide. *Eur. J. Mol. Clin. Med.* **2020**, *7*, 2523–2532.